Application of the Lower Sea Scheldt model in TELEMAC-2D: studying the impact of bridge piers

J. Stark[1], B. De Maerschalck[1]
jeroen.stark@mow.vlaanderen.be, Antwerp, Belgium
[1]Flanders Hydraulics

***Abstract* – The potential impact of the construction of a new cyclist bridge south of Antwerp is studied using a TELEMAC-2D model of the Lower Sea Scheldt. The hydro-morphological impact of the bridge piers is assessed by changes in flow patterns and changes in bottom shear stresses as a result of the pier construction. Exceedance frequencies of a relevant critical shear stress are calculated as well to illustrate potential changes in high- or low-dynamic zones in the study area. Various configurations of bridge piers and support buttresses are tested in a scenario analysis. In addition, several horizontal turbulence model settings are tested in a sensitivity analysis to optimize the representation of the flow patterns and turbulent wakes around the bridge piers.**

Keywords: TELEMAC-2D; bridge piers; Scheldt estuary; horizontal turbulence model.

I. INTRODUCTION

To increase the accessibility of the city of Antwerp for cyclists and to support a modal shift in passenger traffic, the *"OVER THE RING"* project provides for the construction of a new Scheldt bridge for cyclists near the existing Kennedy tunnel just south of Antwerp (Figure 1). This study concerns the hydro-morphological impact of the construction of bridge piers for this new bridge over the Scheldt river in Antwerp, Belgium. A TELEMAC-2D model of the Lower Sea Scheldt, developed by Flanders Hydraulics [1], is applied to study the impact of the bridge piers and quay wall buttresses on the tidal flow patterns in the navigation channel and at the surrounding intertidal flats at the left bank side.

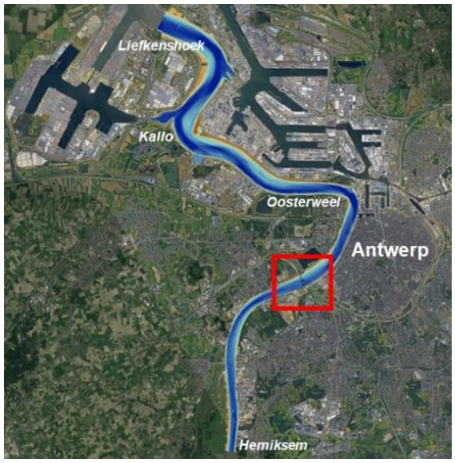

Figure 1. Study area and model domain.

A. Study area

Figure 2 shows the study area just upstream from Antwerp. Along the left bank, the river is surrounded by intertidal mud flats and salt marshes, whereas a vertical quay wall is present along the right bank. The bridge piers are located just upstream of the Kennedy tunnel, recognizable by the protruding levees at the left bank and hence local narrowing of the river width. The most southern main pier is located close to the quay along the right bank, while the other main pier is located centrally in the present fairway. After construction, the main shipping channel will be located between the two main piers, while inland navigation can also move between the left bank and the central pier. The piers are all surrounded by guiding fenders. In addition to the design options with two main bridge piers (i.e., the central and southern pier in Figure 2), several configurations with additional smaller piers closer to the left bank are tested as well. Some of the proposed designs also provide for the construction of an underwater buttress along the existing quay walls at the right bank. These buttresses must stabilize the relatively old quay walls. One of the design options tested in this modelling study also includes an excavation of part of the existing quay to 0 m TAW (i.e., around low water level) along with the construction of a new embankment with a gentle slope of 1:5.

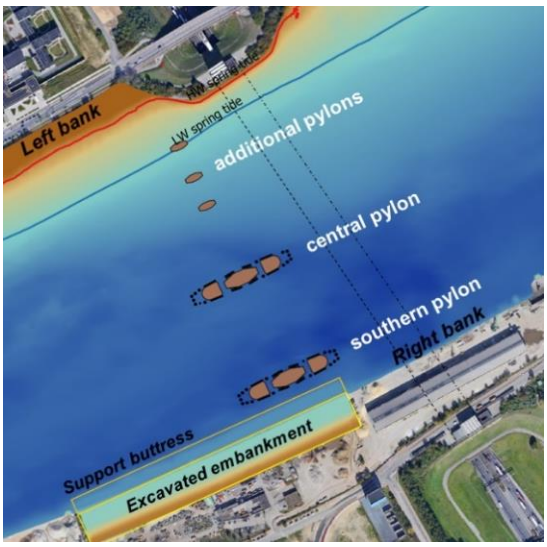

Figure 2. Overview of design scenarios including bridge piers, support buttress and quay wall excavation.

II. MODEL DESCRIPTION

The Lower Sea Scheldt model (here referred to as BZS model) was originally set up by Flanders Hydraulics [1] in TELEMAC-2D (v7p2r2). It covers a 25-km estuary stretch around Antwerp and is forced by observed water level series at both the upstream and downstream boundary. The BZS model has been applied for several hydro-morphological impact studies, including the impact of quay walls, jetties and piers on local flow patterns. This study concerns the potential impact of new bridge piers on flow patterns and tidal flat stability.

The computational mesh of the BZS model was constructed with the advanced triangular mesh generator GMSH [2]. A channel-mesh (structured triangular grid) is applied along the fairway, while adaptive refinement of an unstructured mesh was applied to achieve more accurate predictions at areas of interest or with a complex geometry, such as along the river banks. The total number of elements of the computational grid of the BZS model is approximately 330000 to 350000, depending on the scenario, while the node number varies between 168000 and 180000. The average node distance varies between 10 m and 20 m in the original BZS model without implementation of the bridge piers. However, the resolution is refined up to about 1.5 m in the scenario analysis to adequately implement the piers (Figure 4).

Some numerical settings and physical parameters of the BZS model are included in Table I. For the present analysis, a reduced time-step of 0.5 s was selected after initial testing, ensuring computational stability and accuracy. In particular, longer time-steps induce instabilities at specific dry-wet zones of high spatial resolution (i.e., after mesh refinement at the bridge piers for this scenario analysis). As initial condition, a constant water level equal to 1.57 m TAW is implemented over the entire computational domain. Hence, a hydrodynamic spin-up period of one day is necessary before the model produces relevant output. The relevant simulation period covers one spring-neap tidal cycle (02/04/2018 - 18/04/2018) after this spin-up period. Figure 3 shows modelled water levels at Antwerp for the entire simulation period. The red part of the curve illustrates the spring tide that is selected for the analysis of maximum flood and ebb currents, which provided input for further assessments of the nautical safety [3]. This spring-tide has a tidal range of over 6.5 m at Antwerp, which is considerably higher than the average spring tidal range of 6.0 m. The hydro-morphological impact of the bridge piers is analysed using the full time series (i.e., full spring-neap cycle). This impact is assessed based on maximum velocities, maximum bed shear stresses as well as exceedance probabilities of a critical bed shear stress.

Table I General model settings

Parameter	***Value***
TIME STEP	0.5 s
INITIAL CONDITIONS	constant elevation: 1.57 m
CORIOLIS FORCE	No
SALINITY TRANSPORT	Off
LAW OF BOTTOM FRICTION	Manning (n = 0.018 $m^{1/3}/s$)
OPTION FOR TREATMENT OF TIDAL FLATS	1
TREATMENT OF NEGATIVE DEPTHS	1: smoothing
FREE SURFACE GRADIENT COMPATIBILITY	0.9
TURBULENCE MODEL	5: Mixing length model
SCHEME FOR ADVECTION OF VELOCITIES	1: method of characteristics
SCHEME FOR ADVECTION OF WATER DEPTH	5: conservative scheme
IMPLICATION FOR DEPTH	0.6
IMPLICATION FOR VELOCITIES	1.0
SOLVER	7: GMRES method

A. Calibration and validation

The BZS model was calibrated by tuning bottom friction and varying the turbulence model. The impact of various settings of the turbulence model is discussed in more detail in Section IV. Sensitivity tests indicated that a uniform Manning roughness coefficient of $n = 0.018\ m^{1/3}/s$ could be applied for bottom friction over the entire model domain.

Moreover, the influence of wall friction was assessed by varying the ROUGHNESS COEFFICIENT OF BOUNDARIES between $k_s = 0\ m$ (i.e., smooth wall), $k_s = 0.05\ m$ and $k_s = 1.0\ m$ using the Nikuradse formula. However, no significant differences were noticed between those configurations.

The model was validated for the representation of water levels at the permanent tidal measurement stations at Kallo and Antwerp and for velocity measurements at Oosterweel (see Figure 1 for these locations). Validation shows that the model represents tidal water level variations with a ME and RMSE of

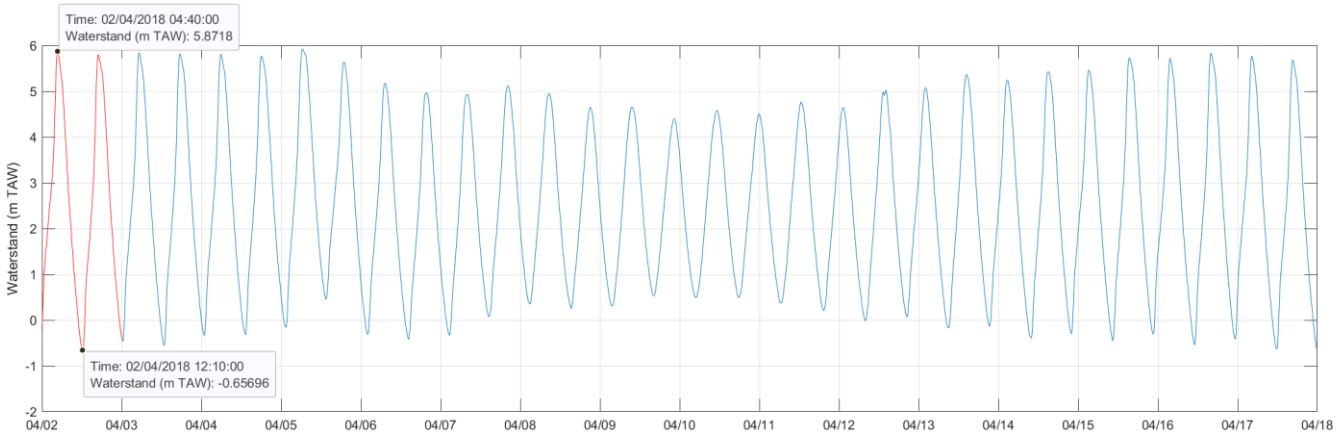

Figure 3. Modelled water level time series at Antwerp.

less than 0.05 m throughout the model domain (Table II). Flow velocities along a sailed ADCP measurement transect and at single-point measurement stations are also represented well. However, ebb velocities at the measurement transect are underestimated near the river banks when the default settings of the mixing length model are applied (Figure 5).

Table II Model validation: water levels

Station	*BIAS [m]*	*RMSE [m]*	*RMSE$_0$ [m]*
Kallo	0.01	0.02	0.02
Antwerpen	-0.03	0.05	0.03

B. Implementation of model scenarios

Table III gives an overview of the various configurations that were tested. Figure 2 shows the locations of the bridge piers as well as the surface area of the excavated right bank that are implemented in these scenarios. For each of the investigated scenarios the computational grid had to be properly adapted and refined in the vicinity of the interventions in order to be aligned with the outline of the proposed constructions (i.e., bridge piers and support buttresses). The refined mesh thus follows the detailed geometry of the piers (Figure 4). For some scenarios, planned excavations of the existing river bank are included by locally expanding the mesh.

Table III Overview of model scenarios

id	*Description*
ref005	*Reference run "present" situation (2018 bathymetry)*
scen012	*two main pylons*
scen023	*two main pylons + excavation and support buttress at right bank*
scen024	*two main pylons + small pylon 1 + excavation and support buttress at right bank*
scen025	*two main pylons + small pylon 2 + excavation and support buttress at right bank*
scen026	*two main pylons + small pylon 3 + excavation and support buttress at right bank*
scen027	*central pylon + excavation and support buttress at right bank*
scen028	*central pylon + small pylon 2 + excavation and support buttress at right bank*

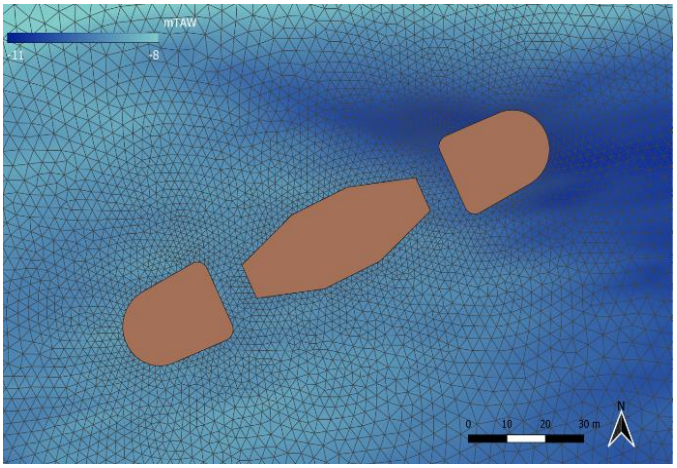

Figure 4. detail of the mesh at one of the bridge piers.

III. RESULTS

The potential impact of the new bridge was assessed by changes in flow patterns (e.g. during maximum ebb and maximum flood) and changes in bottom shear stresses due to the pier construction. As current velocities in very shallow zones and areas that dry up are not very adequately represented in TELEMAC-2D, only model output is used in the analysis for which the water depth in the grid point is at least 1 cm.

In this section, the results of the reference scenario (without bridge piers) and scen023 (i.e., base scenario with two main piers, a support buttress and quay wall excavation along the right bank) are discussed in more detail. The results of all other scenarios with various bridge pier configurations (i.e., combinations of main piers and additional pylons) and different geometries of the support buttresses are available in two Flanders Hydraulics reports [4] and [5].

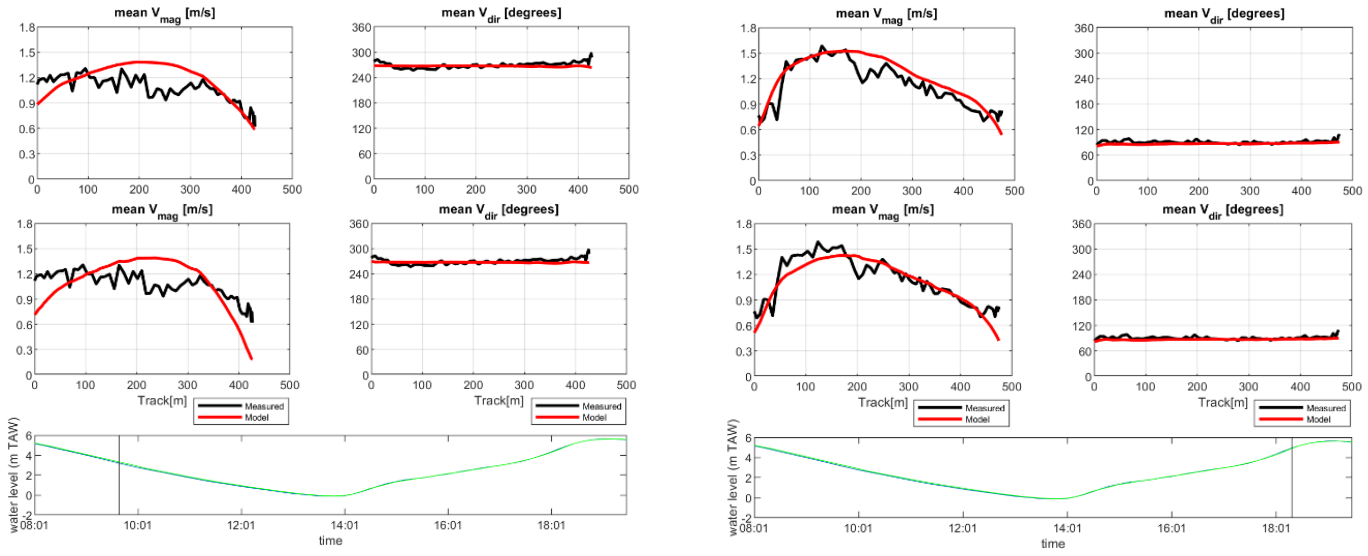

Figure 5. Validation of current velocities at Oosterweel during maximum ebb (left) and maximum flood (right) for two configurations of the horizontal turbulence model: mixing length model with $C_L = 0.26$ (upper panels) and a time- and water level dependent C_L (mid panels).

A. *Hydrodynamic impact*

Figure 6 shows the modelled maximum velocities. The maximum flood current in the study area is significantly higher than the maximum ebb current. In the reference run without bridge piers, peak flow velocities are up to 2.1 m/s during high tide and up to 1.7 m/s during ebb tide. The highest current velocities occur centrally in the river during both high tide and low tide, approximately at the location where the central pier will be constructed.

As a result of the construction of the two bridge piers and the support buttress in scen023, which reduce the cross-sectional area by approximately 10-20% depending on the water level, peak flow velocities in the study area increase to more than 2.4 m/s during maximum flood and more than 1.9 m/s during maximum ebb, with the highest velocities in the middle of the main fairway. In between and around the two main bridge piers, both the ebb current and the flood current increase by +0.2 to +0.3 m/s compared to the current situation.

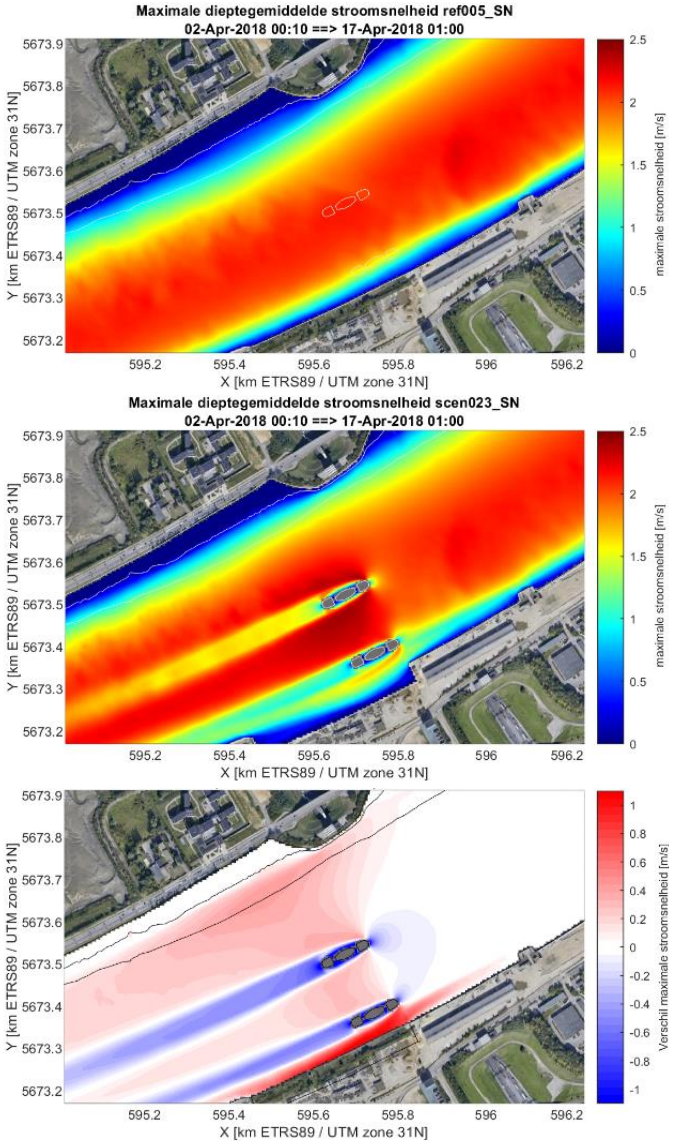

Figure 6. Maximum modelled velocities over a full spring-neap cycle in reference scenario ref005 (top), in scen023 (mid) and the difference (bottom).

There is also a significant increase in maximum flow velocities along the left bank, potentially affecting the intertidal mudflats which are situated there. Just upstream of the Kennedy tunnel, peak flood velocities increase by up to +0.5 m/s during high tide. Ebb flow increases slightly less severe in this area (up to +0.2 m/s). The downstream situated mudflats are less affected as the ebb currents are weaker and due to the sheltering effect of the protruding dike at the Kennedy-tunnel.

Figure 7 illustrates the influence of the support buttress and shallow excavation of the right bank on the maximum speed based on scen023 (i.e., with bridge piers, support buttress and right bank excavation) and scen012 (without support buttress and quay wall excavation). The excavation on the right bank allows for larger tidal flow between the right bank and the southern pier and hence slightly reduces the maximum currents near the left bank. However, the impact of the support buttress and excavation is much less than the impact of the bridge piers themselves.

B. *Morphodynamic impact*

Figure 8 shows the maximum bed shear stresses, as well as the exceedance frequency of a critical shear stress of $\tau_b \geq 1.0\ N/m^2$, both based on the full spring-neap simulation period.

The exceedance frequencies of a relevant critical shear stress are calculated to illustrate potential changes in high- or low-dynamic zones in the study area. In particular, a low exceedance probability of <10% for $\tau_b \geq 1.0\ N/m^2$ approximately coincides with the low-water mark on the left bank (i.e., black contour line in Figure 2) in the reference run (Figure 8). Higher elevated intertidal zones have a lower exceedance frequency, while the subtidal in and the trench are characterized by a higher exceedance frequency. Therefore, an exceedance probability of $\tau_b \geq 1.0\ N/m^2$ will be considered as a proxy for the boundary between intertidal and subtidal areas along the left bank in the scenario analysis.

In scen029, the bed shear stresses and the exceedance probability of $\tau_b \geq 1.0\ N/m^2$ increase in a zone along the left bank, affecting a stretch of approximately 500 m of intertidal flats. There is also an increase in bed shear stresses in the subtidal zone along the left bank, which may imply that protective measures against erosion are necessary in this area.

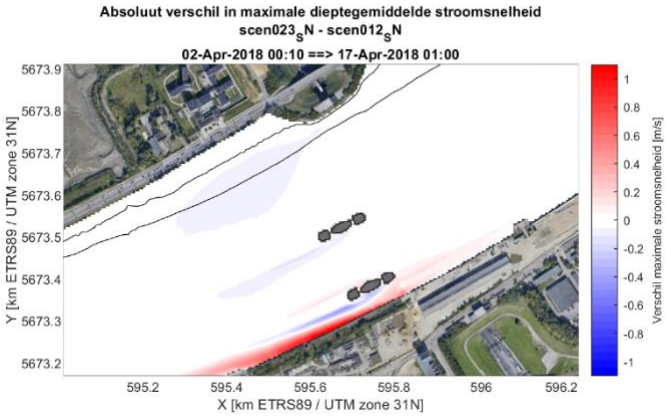

Figure 7. Difference in maximum flow velocities over a full spring-neap cycle between scen023 and scen012.

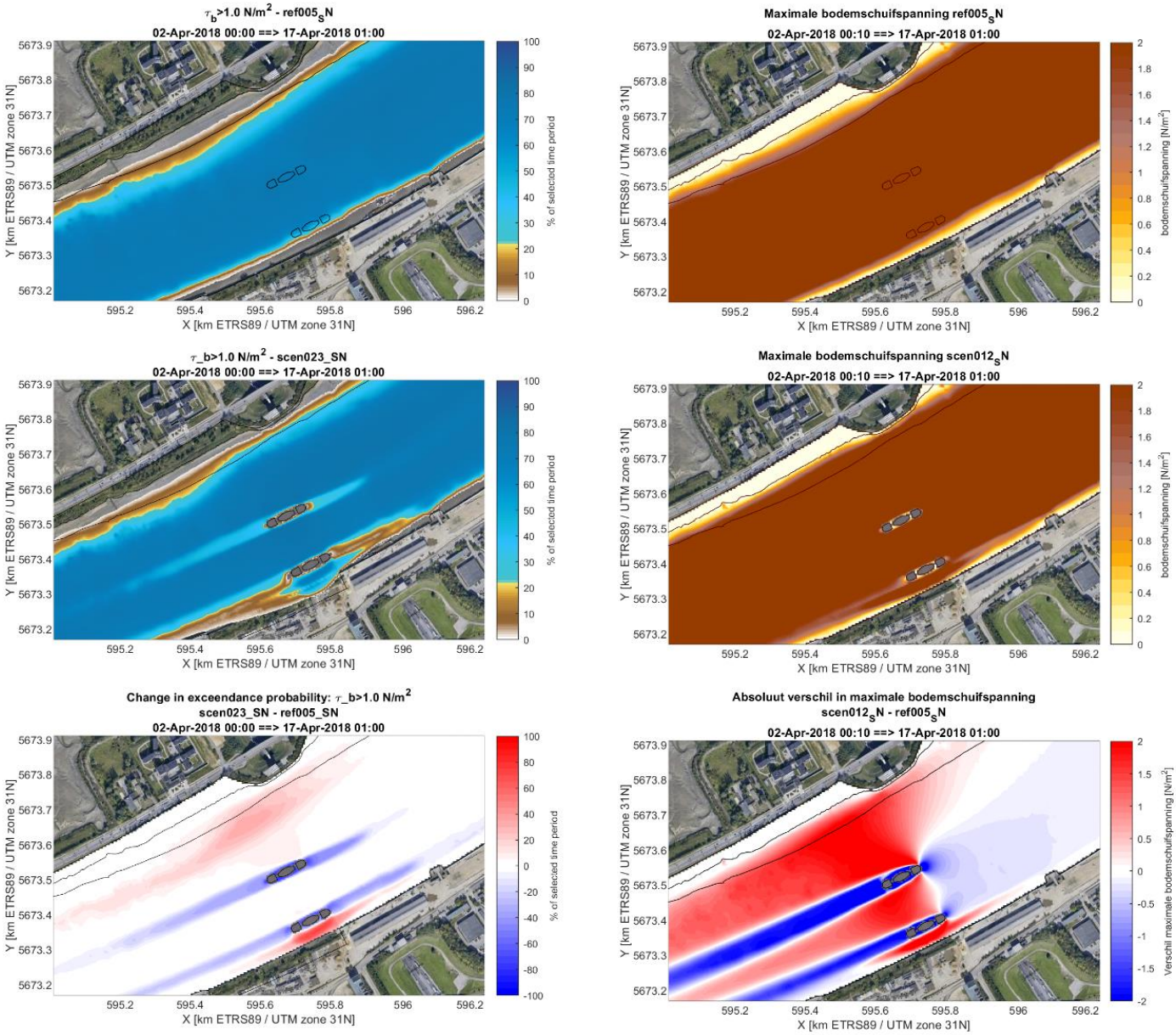

Figure 8. Maximum modelled bed shear stresses (right panels) and exceedance probabilities of a critical bed shear stress of $\tau_b \geq 1{,}0\ N/m^2$ over a full spring-neap cycle in reference scenario ref005 (top panels), in scen023 (mid panels) and the difference (bottom panels).

The impacted zone is mainly situated upstream of the bridge, with the strongest effects parallel to the piers and around the low water line.

Between the two bridge piers, the exceedance frequency of $\tau_b \geq 1.0\ N/m^2$ barely increases, as this zone in the middle of the existing fairway is already characterized by a very high exceedance frequency in the reference situation. However, there is an increase in the maximum bed shear stress, related to higher peak velocities, but further deepening of the main fairway will probably be rather limited due to the presence of less erodible clay layers.

As for the flow velocities, the implementation of the bridge piers causes a strong decrease in the maximum bed shear stresses and the exceedance frequency of $\tau_b \geq 1.0\ N/m^2$ in the wake behind the bridge piers. This wake is present in both upward and downward direction. It should be noted that turbulent flows caused by the fender piers and guiding constructions are not calculated by the current TELEMAC-2D model as they are too small to implement correctly with the applied model resolution and that the structure of the wake could not be validated either. Three-dimensional effects at the foot of the bridge piers, which are typically responsible for erosion pits that are formed around such cylindrical structures, are not simulated either. Finally, the feedback from morphological developments on the hydrodynamics as a result of changed flow patterns is neither calculated. For example, erosive behaviour at the shoal near the left bank can be expected where shear stresses increase. Similarly, zones with decreasing bed shear stresses could accrete. Such

morphological changes may in turn influence current velocities.

IV. SENSITIVITY ANALYSIS: THE HORIZONTAL TURBULENCE MODEL

While calibrating the BZS model, various turbulence models and settings were tested to optimize the model performance and in particular to enhance ebb velocities over the shallow river banks as these were underestimated in the original model validation runs with Prandtl's mixing length model and a constant mixing length coefficient of $C_L = 0.27$ (Figure 5). The depth-averaged mixing length L_m itself is calculated as $L_m = C_L \cdot \kappa \cdot h$, in which C_L is a calibration coefficient with $C_L = 4/15 \approx 0.27$ as default value, κ is the Von Kármán constant and h is the water depth. The model was further calibrated by applying a variable mixing length coefficient C_L. In particular, C_L is configured to remain constant and equal to its default value during flood, and gradually increases up to 10 times its default value, i.e. from $C_L = 0.27$ to $C_L = 2.67$ for free surface elevations lower than 4 m TAW during the ebb phase. The above criterion is regulated by a free surface gradient condition, i.e., based on water depth and water level gradients. It is noted that the high-end values of the time-varying C_L are outside the range of what is considered common in literature (i.e., $0.27 < C_L < 1.25$) [6].

Increasing the mixing length coefficient C_L on shallow areas during ebb leads to higher ebb velocities along the banks and hence improves the representation of the observed tidal flow velocities along the shallow banks at the Oosterweel transect (Figure 4). However, these settings also induced strongly asymmetric flow patterns between flood and ebb at the study site (Figure 9), which were deemed unrealistic. Therefore, several turbulence models and settings are tested in a sensitivity analysis to optimize the model settings for the representation of tidal flow around the bridge piers. Table IV shows some of the configurations that are used to assess the impact of applying various turbulence models to the maximum flood and ebb flow around the bridge piers in the scenario with two large piers and without excavation of the right river bank. These configurations include the mixing length model with various settings for C_L and a simulation with the K-ϵ turbulence model as the mixing length turbulence model does not take into account turbulent kinetic energy transport and dissipation. Finally, a model simulation with a low constant velocity diffusivity is carried out as well.

These sensitivity tests show that the mixing length model with default settings and the K-ϵ model with lead to very similar results. Despite the fact that C_L is only increased in the shallow parts during ebb, Figure 9 shows that applying the time-varying C_L has a significant impact on the flow around the piers during ebb current. In this configuration, the flow around the piers becomes strongly asymmetric between ebb and flood (i.e., for similar ebb and flood velocities), while there is no physical explanation for this asymmetry. On the other hand, when applying a constant C_L or the K-ϵ model, the flow pattern around the piers is more comparable between ebb and flood. As scen012 with the default settings of the mixing length model leads to more reliable results than scen009 with variable C_L and also gives the more stable results than scen015 with the K-ϵ model, this configuration is eventually applied in the present scenario analysis.

Table IV Overview of sensitvity tests.

id	*Description*
scen009	Mixing length model (C_L time/depth-dependent)
scen012	Mixing length model (C_L = 0.27; TELEMAC-2D default)
scen013	Mixing length model (C_L = 2.67)
scen014	Mixing length model (C_L = 1.25; maximum according to [6])
scen015	K-ϵ turbulence model
scen016	CONSTANT VELOCITY DIFFUSIVITY = 0.005

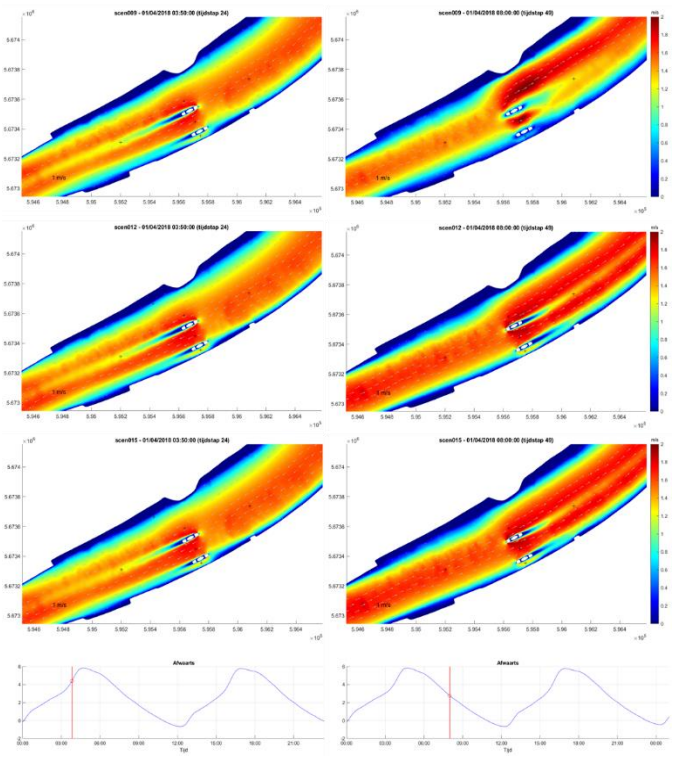

Figure 9. Modelled typical flow patterns at the bridge piers during flood (left) and ebb (right) for scen009 (top), scen012 (mid) and scen015 (bottom).

A. *Oscillating vortex streets*

In the above simulations, no oscillating Von Kármán vortices are noticeable in the wake behind the bridge piers. It is known that shallow water solvers based on finite element methods, such as TELEMAC-2D, induce numerical diffusion which tends to smooth out any vortices in the wake due to additional diffusion in the momentum equation [7]. Nevertheless, additional sensitivity tests with a CONSTANT VELOCITY DIFFUSIVITY = 0.005 in scen016 allow for the reproduction of oscillating Von Kármán vortices behind the bridge piers (Figure 10) as the additional diffusivity induced by the turbulence model is now limited to a relatively low value. The size and frequency of these vortices could not be validated due to a lack of measurements at similar sites along the Scheldt river. From literature, it is known that the formation of oscillatory vortices behind piers or pylons is highly dependent

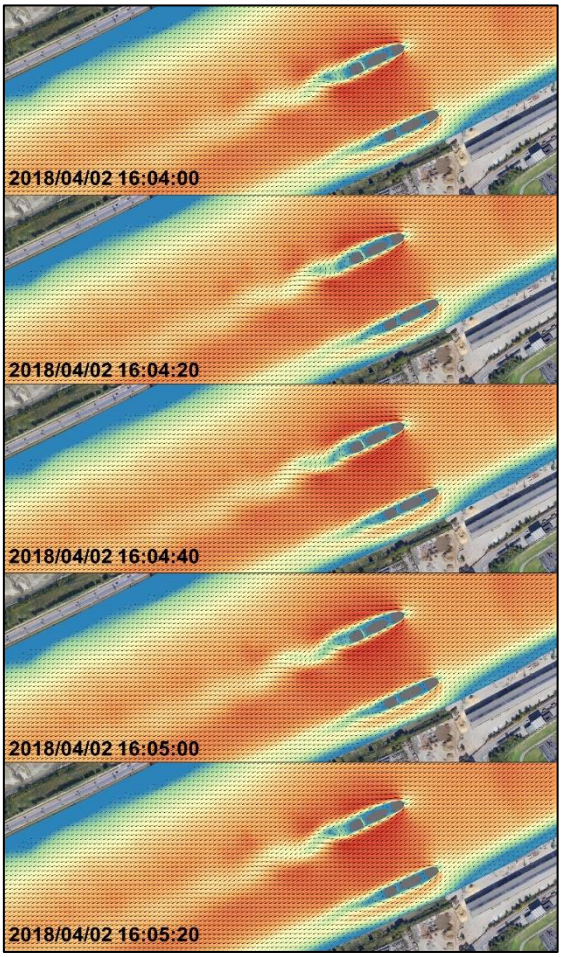

Figure 10. Oscillating Von Kármán vortices in scen016 with CONSTANT VELOCITY DIFFUSIVITY = 0.005.

on the shape of these piers as well as on the Reynolds number ($R_E = V \cdot d \cdot v^{-1}$, with V the undisturbed upward velocity, d the characteristic length related to the diameter of the pier and v the kinematic viscosity). For comparison, for a cylindrical pier with a diameter of 20 m and a flow velocity of 1.0 m/s, the Reynolds number is approximately $15 \cdot 10^6$, which should induce a turbulent flow with or without an oscillating character.

V. CONCLUSIONS

The potential impact of the construction of bridge pylons for a new cyclist bridge south of Antwerp was studied using the BZS model. The hydro-morphological impact was assessed by changes in flow patterns and changes in bottom shear stresses due to the pylon construction. Exceedance frequencies of a relevant critical shear stress were calculated as well to illustrate potential changes in high- or low-dynamic zones in the study area.

The implementation of the bridge pylons induces an increase in current velocities in the fairway during both ebb and flood. Contrastingly, flow velocities actually decrease in the wake behind the pylons, causing more cross-sectional variation in current velocities. The reduction of the cross-sectional area as a result of the construction of the bridge pylons also enlarges the maximum flow over the intertidal flats along the left bank. The construction of an underwater buttress to protect the quay wall along the right bank has a much more limited influence than the bridge pylons themselves.

A sensitivity analysis for the influence of the horizontal turbulence model indicates that the (turbulent) structure and length of the wake behind the pylons is very sensitive to the applied settings of the horizontal turbulence model. Typical Von Kármán vortices could only be represented using a low constant diffusivity coefficient. It should be noted that the 2D character of the model would only allow for an accurate representation of the wake if vortex shedding is present according to [8]. Moreover, the BZS model resolution does not include all details of the pylons, such as the support fenders along the piers, individual piles in front of the bridge piers, or the pile construction under the collision protection. All these structural elements determine the turbulence induced by the bridge piers and thus the structure of the wake. Ultimately, the computed flow patterns are also used as input for the Flanders Hydraulics ship manoeuvring simulator [3]. Depending on the results of the nautical simulation study, it may be appropriate to model the length of the wake and the possible turbulent vortices in the wake behind the piers in more detail using a CFD (Computational Fluid Dynamics) simulation or a physical scale model.

REFERENCES

[1] G. Kolokythas, S. Smolders, B. De Maerschalck, F. Mostaert, “Accessibility INEOS Oxide jetty: sub report 3. Development of a high-resolution 2D hydrodynamic model for the Lower Sea Scheldt,” FHR reports, 19_075_3. Flanders Hydraulics Research: Antwerp, 2020.

[2] C. Geuzaine, J.-F. Remacle, “Gmsh: a three-dimensional finite element mesh generator with built-in pre-and post-processing facilities,” Int. J. Numer. Methods Eng. 79(11), 2009, pp. 1309–1331.

[3] K. Eloot, J. Verwilligen, “Antwerpen Oeververbinding tussen linker- en rechteroever: Deelrapport 3 – Simulatiestudie invloed brugpijlers en onderwatertalud rechteroever,” FHR reports, 21_113_3. Flanders Hydraulics Research: Antwerp, 2022.

[4] J. Stark, B. De Maerschalck, “Antwerpen Oeververbinding tussen linker- en rechteroever: Deelrapport 2 – Hydrodynamische modellering brugpijlers,” FHR reports, 21_113_2. Flanders Hydraulics Research: Antwerp, 2023.

[5] B. De Maerschalck, J. Stark, K. Eloot, “Antwerpen Oeververbinding tussen linker- en rechteroever: Deelrapport 4 – Hydrodynamische beoordeling ontwerpvarianten,” FHR reports, 21_113_4. Flanders Hydraulics Research: Antwerp, 2023.

[6] C. Dorfmann, G. Zenz, “The depth-averaged Mixing Length turbulence model for Telemac-2D,” In: Proceedings of the XXIIIrd TELEMAC-MASCARET User Conference 2016, 11 to 13 October 2016, Paris, France., 2016, pp. 163-168..

[7] C. Kessler, U. Merkel, “Vortex streets behind bridge piers, studies with TELEMAC 2D/3D & TELEMAC AD”, In: Proceedings 23rd TELEMAC & Mascaret User Club, Paris, 2017.

[8] P.K. Stansby, “Limitations of Depth-Averaged Modeling for Shallow Wakes,” Journal of Hydraulic Engineering (ASCE), 132, 2006, pp. 737-740.